

This is an Open Access document downloaded from ORCA, Cardiff University's institutional repository:<https://orca.cardiff.ac.uk/id/eprint/139393/>

This is the author's version of a work that was submitted to / accepted for publication.

Citation for final published version:

Guo, Tianxiao, Yang, Nianjun, Yang, Bing, Schulte, Anna, Jin, Qun, Koch, Ulrike, Mandal, Soumen , Engelhard, Carsten, Williams, Oliver A. , Schönherr, Holger and Jiang, Xin 2021. Electrochemistry of nitrogen and boron bi-element incorporated diamond films. Carbon 178 , pp. 19-25.
10.1016/j.carbon.2021.02.062

Publishers page: <http://dx.doi.org/10.1016/j.carbon.2021.02.062>

Please note:

Changes made as a result of publishing processes such as copy-editing, formatting and page numbers may not be reflected in this version. For the definitive version of this publication, please refer to the published source. You are advised to consult the publisher's version if you wish to cite this paper.

This version is being made available in accordance with publisher policies. See <http://orca.cf.ac.uk/policies.html> for usage policies. Copyright and moral rights for publications made available in ORCA are retained by the copyright holders.



Electrochemistry of Nitrogen and Boron

Bi-element Incorporated Diamond Films

Tianxiao Guo,^a Nianjun Yang,^{a*} Bing Yang,^b Anna Schulte,^c Qun Jin,^a Ulrike Koch,^d
Rainer Bornemann,^e Soumen Mandal,^f Carsten Engelhard,^d Oliver A. Williams,^f
Holger Schönherr,^c and Xin Jiang^{a,*}

^a Institute of Materials Engineering, University of Siegen, Siegen 57076, Germany

^b Shenyang National Laboratory for Materials Science, Institute of Metal Research
(IMR), Chinese Academy of Science (CAS), No. 72 Wenhua Road, Shenyang
110016, China

^c Physical Chemistry I, Department of Chemistry and Biology and Research Center of
Micro and Nanochemistry and Engineering (Cμ), University of Siegen, Siegen 57075,
Germany

^d Analytical Chemistry, Department of Chemistry and Biology and Research Center
of Micro and Nanochemistry and Engineering (Cμ), University of Siegen, Siegen
57075, Germany

^e Institute for High Frequency and Quantum Electronics, School of Science and
Technology, University of Siegen, Siegen, Siegen 57076, Germany

^f School of Physics and Astronomy, Cardiff University, Cardiff CF24 3AA, UK

* Corresponding author. Tel: 0049271 7402531 (N. Yang); 0049 271740-2966 (X.
Jiang)

E-mail: xin.jiang@uni-siegen.de (X. Jiang); nianjun.yang@uni-siegen.de (N. Yang)

Abstract (188 words)

Boron doped diamond (BDD) has been widely used in various electrochemical fields, due to its unique physical and chemical properties. However, the investigation of the electrochemistry of bi-element incorporated diamond, especially the variation of surface components after nitrogen incorporation into BDD and the corresponding electron transfer of inner-sphere and outer-sphere redox probes is still lacking. Here, the electrochemistry of nitrogen and boron bi-element incorporated diamond (NBD) is thus investigated in both inner and outer redox systems, namely in $[\text{Fe}(\text{CN})_6]^{3-/4-}$ and $[\text{Ru}(\text{NH}_3)_6]^{3+/2+}$ solutions. On the NBD electrode, enhanced electrochemical responses are achieved for both outer- and inner-sphere redox reactions. Such enhancement originates from the enrichment of C=O groups and the increased amount of sp^2 species in the NBD film. Moreover, the nitrogen and boron atoms incorporated in diamond modulate the surface polarities and the electronic states of diamond. Based on the enhanced and stable capacitance of the NBD electrode, its electrochemical energy applications are explored by assembling its supercapacitor as a case study. This work reveals the influence of sp^2 species and oxygen-contained function group on the electrochemistry of bi-element incorporated diamond films and reveals their potential electrochemical applications.

Keywords: Electrochemistry, nitrogen and boron-doped diamond, sp^2 -carbon

1. Introduction

The electrochemistry of doped diamond, especially p-type diamond or boron doped diamond (BDD) has been widely investigated in the past decades. As an excellent electrode material, BDD has been utilized for electrochemical sensors [1, 2], supercapacitor construction [3-5], CO₂ reduction [6, 7], nitrogen redox reaction (NRR) [8], and wastewater treatment [9, 10]. These applications originate from the unique features of a BDD electrode, such as its low background current, wide potential windows in different media, and long-term durability. Boron atoms doped in diamond realize the transformation of diamond from an intrinsic insulator to a semiconductor [11], and finally to a metal-like conductor once the boron doping level increases above to 10²⁰ cm⁻³ [12]. It is well-known that the diamond crystal structure, surface termination, and sp² species or sp²/sp³ ratio on the diamond surface play significant roles to determine the electrochemical features of a BDD electrode. For example, a rough BDD surface promotes the transformation of the Faradaic reactions from kinetic- to diffusion-control together with enhanced charge transfer rates [13, 14]. The surface (e.g., hydrogen, oxygen) terminations of a BDD film influence the kinetics of Faradaic reactions on the diamond surface because these terminations possess significant difference in their electronic structures [15-17]. In this regard, the electrochemistry of BDD films containing various amounts of sp² carbon has been also extensively studied, although their quality is much reduced and their background currents are much enhanced [18]. To further boost the performance of diamond films in the fields of energy and

1 catalysis applications, diamond composite structures have been designed, for instance
2 to assemble battery-like supercapacitors by use of aligned carbon nanofiber coated
3 BDD [4], to achieve an efficient methanol oxidation reaction (MOR) using nanoporous
4 platinum particles coated BDD [19].

5 On the other hand, electrochemistry of n-type diamond, namely diamond films doped
6 with nitrogen or phosphorus atoms has also attracted much attention. Nitrogen doping
7 or incorporation into carbon materials has also been confirmed as a fruitful strategy to
8 promote the electrocatalytic activity of these carbon materials. The pyridinic N atoms
9 create Lewis basic sites that are actually regarded as the catalytic active sites [20, 21].

10 For example, a nitrogen doped diamond (NDD) film is proved to contain N-sp³
11 components, namely electrocatalytic active sites [22, 23]. In this context, a NDD film
12 exhibits high overpotential for the hydrogen evolution reaction (HER) and has been
13 applied for highly efficient CO₂ reduction [24, 25].

14 We are interested in the electrochemistry of bi-element incorporated diamond films.
15 Compared with diamond films doped with a single dopant, diamond films with dual
16 dopants are expected to regulate the electronic structure of diamond materials and
17 eventually exhibit faster electron transfer rates and more active sites for catalysis [26-
18 28]. Such enhanced electrochemical performance stems from the synergistic effects of
19 two different and incorporated atoms in the diamond film. One recent example is the
20 application of nitrogen and boron co-doped diamond (NBD) film for the efficient CO₂
21 reduction [29]. The NBD film with optimized contents of nitrogen and boron dopants

exhibited comparable performance toward oxygen reduction reaction (ORR) to the Pt/C catalyst, including a high current density for ORR and long-term durability of the system [30]. In spite of these successful catalytic applications of these bi-element incorporated diamond films, the electrochemistry of the NBD films has been seldom investigated. For example, the variation of surface components in the NBD films and their influence on the electron transfer rates of both inner-sphere and outer-sphere redox systems have not been clarified up to now. Moreover, reports about the applications of bi-element incorporated diamond films for energy storage are still missing in the literature, although BDD and its composites are shown to be promising electrode candidates for the assembly of supercapacitors [4, 31, 32]. Therefore, this contribution deals with the electrochemistry of the NBD films that are grown by a microwave plasma enhanced chemical vapor deposition (MPCVD) method. After the characterization of this NBD film with different techniques, its electrochemical responses are studied in both $[\text{Fe}(\text{CN})_6]^{3-/4-}$ and $[\text{Ru}(\text{NH}_3)_6]^{3+/2+}$ redox systems, which are further compared with the BDD electrode. As a case study of the energy applications of these NBD films, a supercapacitor is assembled and investigated.

2. Experiment section

2.1 Materials synthesis and characterization

The NBD and BDD films were grown on the Si (100) wafers using a MPCVD method [33-35]. The detailed growth parameters are listed in **Table S1**.

The SEM images of the as-grown NBD and BDD films were recorded with a field emission scanning electron microscope (FESEM, Zeiss ultra55, Germany). The transmission electron microscopy (TEM, FEI G² F20) was employed to characterize the defects the crystalline defects in the as-grown NBD and BDD films. The surface chemical composition of these as-grown diamond films was analyzed by X-ray photoelectron spectroscopy (S-probe ESCA SSX-100s, Surface Science Instruments, USA) with an Al K α radiation of 200 W. The survey spectra were measured from 0 to 1200 eV with a resolution of 1 eV at a spot size of 800 μm^2 . The high resolution spectra were collected with a resolution of 0.1 eV at a spot size of 300 μm^2 . The Raman spectra of the as-grown diamond films were collected on a homemade Raman Instrument equipped with a 532-nm laser. A time-of-flight secondary ion mass spectrometer (ToF-SIMS IV, ION-TOF GmbH, Germany) was used to map the dopants in these as-grown diamond films, such as the contents of nitrogen and boron atoms in the NBD films as well as boron atom in the BDD film. For these mapping experiments, a 25-keV Bi⁺ primary ion beam was employed to bombard the diamond surface within an area of 300 \times 300 μm^2 .

2.2 Electrochemical measurements

Electrochemical measurements of the as-grown NBD and BDD films were conducted on a CHI660e workstation (Shanghai Chenhua Inc., China) using a three-electrode cell, where an Ag/AgCl (3MKCl) electrode acted as reference electrode, a Pt wire as counter

electrode, a NBD film or a BDD film as working electrode. The geometric area of a working electrode was 0.05 cm^2 . To investigate the electrochemical performance of the NBD and BDD films, their cyclic voltammograms (CVs) were recorded in either 1 mM $\text{K}_3[\text{Fe}(\text{CN})_6]$ or $[\text{Ru}(\text{NH}_3)_6]\text{Cl}_3$ dissolved in 1 M KCl aqueous solution. The investigation of the pseudocapacitive behavior of the post-treated NBD and BDD films was carried out by means of cyclic voltammetry at different scan rates and by means of the galvanostatic charge/discharge (GCD) method at different current densities. The post-treatment was conducted in the mixture of H_2SO_4 and HNO_3 (V/V = 3:1) for 30 min. In this way, these diamond films were found to exhibit better wettability in the electrolytes. The electrolyte used for the assemble of a supercapacitor was 0.05 M $\text{K}_3\text{Fe}(\text{CN})_6/\text{K}_4\text{Fe}(\text{CN})_6$ dissolved in 1.0 M Na_2SO_4 solution. The specific capacitances were calculated according to the reported methods [4, 36]. The calculation of the contribution of the capacitive current was based on the equation of $i(V) = k_1v + k_2v^{1/2}$ [37, 38]. Here, $i(V)$ is the related current at the potential of V, v is scan rate, $k_2v^{1/2}$ and k_1v are related to diffusion-controlled and capacitive-controlled, respectively. Note that the capacitive current can be also evaluated directly from the cyclic voltammograms (CVs) or the GCD curves in the blank solutions (namely those containing only supporting electrolytes).

3. Results and discussion

3.1 Characterization of the NBD films

1 The morphologies of the as-grown BDD and NBD films were analyzed by electron
2 microscopy. From the typical SEM images of the NBD (**Figure 1a**) and BDD (**Figure**
3 **S1**) films, one can see clearly that these films exhibit typical and similar morphology
4 to that of polycrystalline diamond films. Their grain sizes are in the range of 0.4 - 1.2
5 μm . The cross-sectional SEM images of the NBD and BDD films (**Figure S2**) reveal
6 their thickness to be about 1.5 μm . To check out crystalline defects on these films, the
7 TEM images of the NBD film were recorded (**Figure 1b, 1c**), where twin boundaries
8 and stacking faults are observed. The presence of these defects is caused by the
9 incorporation of both nitrogen and boron atoms into the diamond film. At selected
10 locations for TEM imaging experiments, it seems to be that the crystalline defects of
11 the NBD film are reduced, compared to the BDD film (**Figure S1**). Meanwhile, the
12 crystalline quality of a NBD film seems to be improved and the {100} texture of
13 diamond is promoted [39]. In a high-resolution TEM (HRTEM) image of a NBD film
14 (**Figure 1c**), the atomic structure of the NBD film can be clearly seen along the [01-1]
15 zone axis. According to the inset of fast Fourier transformation (FFT), the diffraction
16 spots reveal spacings of 0.206 and 0.18 nm. These spacings correspond to the (111) and
17 (200) planes of diamond phase, respectively. Consequently, the as-grown NBD and
18 BDD films exhibit high crystallinity.

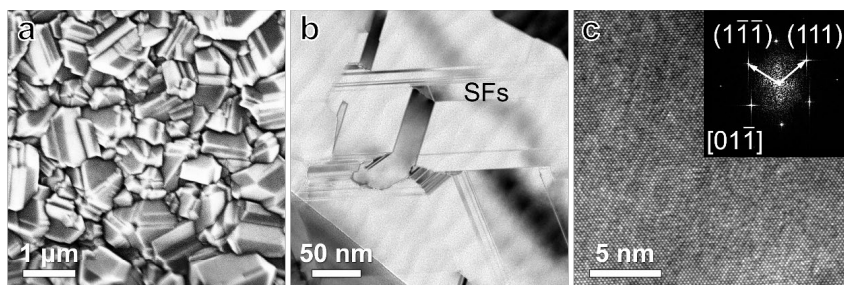


Figure 1. (a) SEM, (b) low-magnification TEM and (c) HRTEM images of a NBD film.

The inset in (c) is the corresponding fast Fourier transformation (FFT) of the HRTEM image.

The Raman spectra of the as-grown NBD and BDD films were also recorded (**Figure 2a**). In both spectra, the typical Raman peak of diamond is seen around 1320 cm^{-1} . The Lorentzian peak located around 1200 cm^{-1} is classified as the symmetry breaking of the diamond lattice. The spectrum of a NBD film displays a finite blueshift, resulting from a higher bond energy when nitrogen and boron atoms are bi-element incorporated in the diamond lattice [40]. Moreover, both Raman spectra of the as-grown NBD and BDD films reveal a broad peak around at 1580 cm^{-1} . It is known as the G band that results from the bond stretching of sp^2 atoms in both rings and chains.

To determine the surface chemical bonding of the as-grown NBD and BDD films, their survey and C1s XPS spectra were recorded and compared (**Figure S3 and Figure 2b**). In both XPS spectra, four peaks centered at 282.8, 284.1, 285.2, and 286.3 eV are attributed to sp^2 and sp^3 hybridized carbon species, as well as carbon bonded to oxygen as C–O and as C=O, respectively [41, 42]. The peak located around 284.8 eV in the

NBD film corresponds to carbon bonded to nitrogen. Furthermore, it can be seen that the NBD film reveals a substantially higher sp^2/sp^3 ratio than the BDD film together with an increased fraction of carbon in C=O and C-O bonds (Table S2). The nitrogen atoms incorporated into diamond are expected to be three-fold coordinated in the amorphous/disordered regions with the remaining electrons in a lone pair configuration. In other words, the nitrogen atoms incorporated into diamond promotes the formation of sp^2 carbon [43, 44]. Under such conditions, nitrogen incorporation into diamond tends to change the bonding, instead of being assimilated by the diamond lattice that is not the intrinsic of electronic dopant. Figure 2c shows that the B1s peak of the NBD film is shifted to a lower binding energy compared to the B1s peak of the BDD film. Presumably, this is due to the formation of B-N bonds in the NBD film. In the N1s XPS spectrum of the NBD film (Figure 2d), two peaks are detected at 399.7 and 397.5 eV, which are attributed to nitrogen atoms bonded to carbon and to boron, respectively [25, 29, 30]. In the XPS spectrum of the BDD film, no N1s peak was detected. The ratios of nitrogen to carbon and boron to carbon were estimated from the high resolution XPS spectra of the NBD film. They are 0.013 and 0.008, respectively. Similarly, the ratio of boron to carbon in the BDD film is 0.008. Furthermore, boron atoms are found to be homogeneously and uniformly distributed throughout the film, as confirmed from secondary ion mass spectrometry (SIMS) mappings of doped boron atoms in the NBD and BDD films (Figure 2e, 2f, S4). Surprisingly, nitrogen was not detectable with the current SIMS setup, due to isobaric interferences from carbon species with similar

mass-to-charge ratios (m/z) (Figure S4 a-b). Meanwhile, the content of incorporated nitrogen in the NBD film under investigation is presumably not very high (e.g., less than 10^{18} atoms cm^{-3}) and close to or at the detection limit of our SIMS setup. In the future, a better primary beam intensity and improved vacuum will help to achieve improved detection limits for incorporated nitrogen atoms in these NBD films.

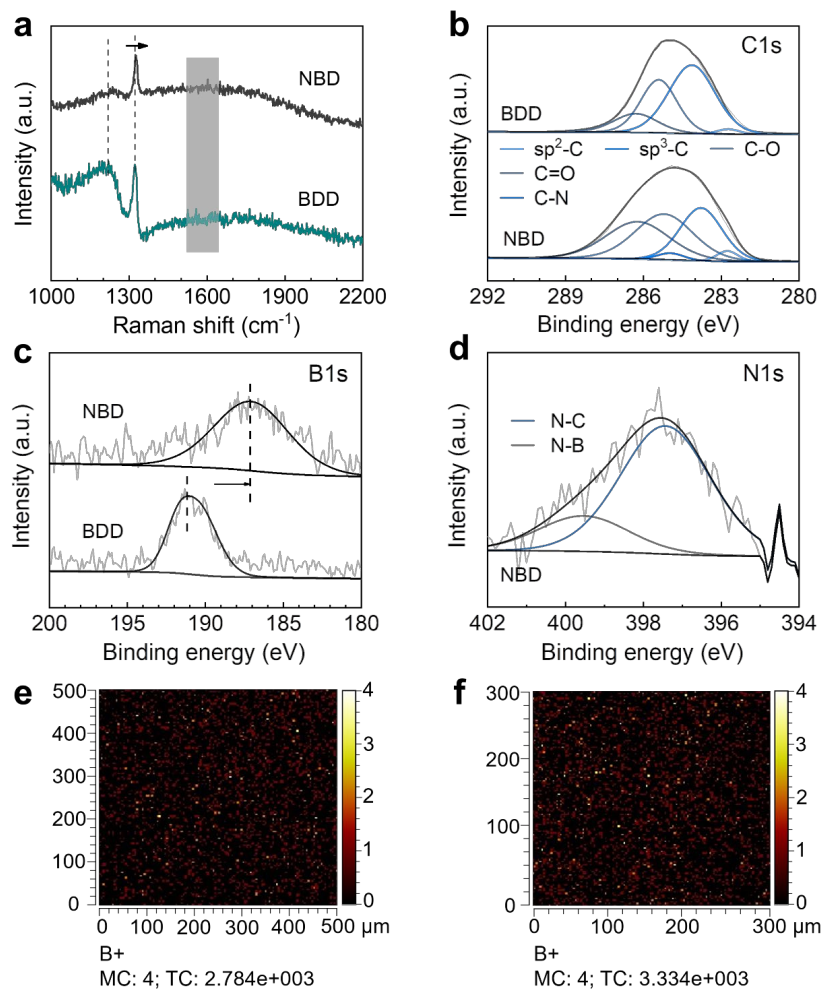


Figure 2. (a) Raman spectra of the NBD and BDD films; their C1s (b), B1s (c) and N1s (d) XPS spectra; SIMS mapping of boron atoms doped in the NBD film directly (e) and after 30 sec sputtering with Argon for cleaning the surface (f) in the positive ion mode (MC max counts per pixel, TC total counts).

3.2 Electrochemical properties of the NBD films

The electrochemistry of the as-grown NBD and BDD films was then investigated and compared. Both inner and outer redox systems were used, namely 1 mM $[\text{Ru}(\text{NH}_3)_6]\text{Cl}_3$ (**Figure 3a**) and 1 mM $\text{K}_3[\text{Fe}(\text{CN})_6]$ (**Figure 3b**) dissolved in 1 M KCl aqueous solution. For the $[\text{Ru}(\text{NH}_3)_6]\text{Cl}_3$ redox system (**Figure 3a**), the NBD electrode shows a higher peak current (e.g., a cathodic peak current, $I_c = 140.22 \mu\text{A cm}^{-2}$) and a bigger difference of peak separation ($\Delta E_p = 72 \text{ mV}$) than the BDD electrode ($I_c = 131.08 \mu\text{A cm}^{-2}$ and $\Delta E_p = 58 \text{ mV}$). For the $\text{K}_3[\text{Fe}(\text{CN})_6]$ redox system (**Figure 3b**), I_c rises from $145.5 \mu\text{A cm}^{-2}$ on a BDD electrode to $162.34 \mu\text{A cm}^{-2}$ on a NBD electrode. However, a NBD electrode shows a bigger ΔE_p (84 mV) than a BDD electrode (75 mV). As inner-sphere redox probes, the electrode kinetics of $[\text{Fe}(\text{CN})_6]^{3-/4-}$ is known to be tightly related to surface terminations or surface functional groups of a diamond electrode [42]. Different from the $[\text{Fe}(\text{CN})_6]^{3-/4-}$ inner-sphere redox system, the electron transfer and the electrode kinetic of the outer-sphere $[\text{Ru}(\text{NH}_3)_6]^{3+/2+}$ redox system is influenced mainly by the carrier density (e.g., the amount of sp^2 carbon species) of the diamond films [17, 45]. According to the growth parameters, the NBD and BDD films feature high boron

densities or low electricity that is favorable for fast electron transfer processes [16]. However, a higher amount of boron atoms is expected to be doped in the NBD film than that in a BDD film. This originates from the "enhanced incorporation" effect of nitrogen in the gas mixture. The XPS results showed that the NBD film is enriched in C=O bonds compared to the BDD film. These surface oxygen groups on the electrodes thus block electrochemical active sites of the NBD electrode and/or bring more repulsive force for the negatively charged $[\text{Fe}(\text{CN})_6]^{3-/4-}$ redox probes to interact with the NBD electrode. The electron transfer process of $[\text{Fe}(\text{CN})_6]^{3-/4-}$ redox probes is thus inhibited on the NBD surface, eventually leading to reduced peak currents. On the other hand, the increased amount of sp^2 species after the nitrogen incorporation into a BDD film leads to the decrease of carrier density that promotes the electron transfer of outer-sphere $[\text{Ru}(\text{NH}_3)_6]^{3+/2+}$ redox probes and finally more pronounced peak currents.

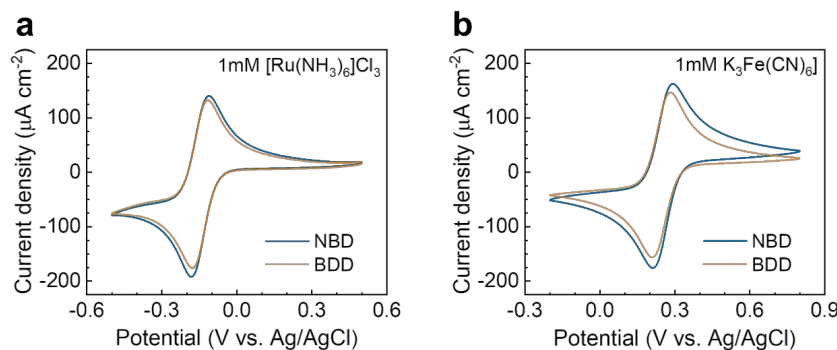


Figure 3. Cyclic voltammograms of the NBD and BDD electrodes at a scan rate of 0.1 V s^{-1} in (a) 1 mM $[\text{Ru}(\text{NH}_3)_3]\text{Cl}_3$ and (b) 1 mM $\text{K}_3\text{Fe}(\text{CN})_3$ dissolved in 0.5 M KCl solution.

3.3 Electrochemical applications of the NBD films

To explore the electrochemical applications of such NBD films, they were utilized as the capacitor electrodes for the supercapacitor assembly. In such a case study, these NBD films were wet-chemically treated since such post-treatment improved much their wettability. Here, a redox-electrolyte enhanced supercapacitor was fabricated [4, 46]. From the CVs of the NBD and BDD films recorded at different scan rates (Figure S6), one can notice stable ΔE_p and I_c at all scan rates. These results indicate the perfect reversibility of the NBD and BDD films or these diamond capacitor electrodes in such an electrolyte. Notice here that the ΔE_p values in Figure S5 are different from those in Figure 3b, although the used redox electrolytes are same. This is because these diamond electrodes in Figure S5 were wet-chemically treated, while those in Figure 3b were the as-grown diamond films. In other words, different surface terminations on these electrodes affect significantly the kinetics of redox reactions on these diamond electrodes [15-17]. The estimated capacitances of the NBD electrode are 87.7, 66.8, 39.4, and 26.8 mF cm⁻² at the scan rates of 10, 20, 50, and 100 mV s⁻¹, respectively. Meanwhile, the galvanostatic charge/discharge (GCD) curves of the NBD and BDD electrodes (Figure 4a) also reveal good reversibility, as confirmed from the almost equal charge and discharge times in these GCD curves. The calculated capacitances of the NBD electrode (Figure 4b) are 98.9, 56, 28.7, and 14.9 mF s⁻¹ at the current densities of 1, 2, 4, and 8 mA cm⁻², respectively. They are higher than those of a BDD electrodes: 71.3, 39.7, 20.8, and 10.7 mF s⁻¹ at the current densities of 1, 2, 4, and 8 mA

cm², respectively. The capacitive contribution of the NBD and BDD electrodes were further calculated to explore the difference of the reaction kinetics between two capacitor electrodes. **Figure 4c** presents the contribution ratios of capacitive-controlled and diffusion-controlled processes on the NBD and BDD electrodes. Both exhibit an increased ratio of capacitive contribution with the enlargement of scan rate. Specifically, the NBD electrode shows a higher capacitive contribution ratio than a BDD electrode. This reveals the underlying essence of the better rate performance of the NBD electrode. The enhanced capacitance of the NBD electrode is because the incorporation of nitrogen and boron atoms into diamond modulates the surface polarities and the electronic of materials [47, 48]. For example, the charge-transfer resistance of the NBD film, as estimated from its Nyquist plots (**Figure S7**) is 94 Ω, which is smaller than that (143 Ω) of the BDD film.

The long-term cycling stability of the BDD and NBD electrodes was further tested at the current density of as high as 8 mA cm⁻². Although the NBD electrode exhibits a higher capacitance than a BDD electrode, both electrodes show the similar cycling stability even after 10000 GCD cycles (**Figure 4d** and **Figure S8**). All these results confirm the suitability of employing the NBD film for electrochemical energy storage applications. Note that the surface of the post-treated NBD electrode is possible to be re-activated electrochemically or by use of a plasma technique. The studies on the effect of the surface terminations of the NBD electrode on their capacitive performance are currently undergoing in our lab.

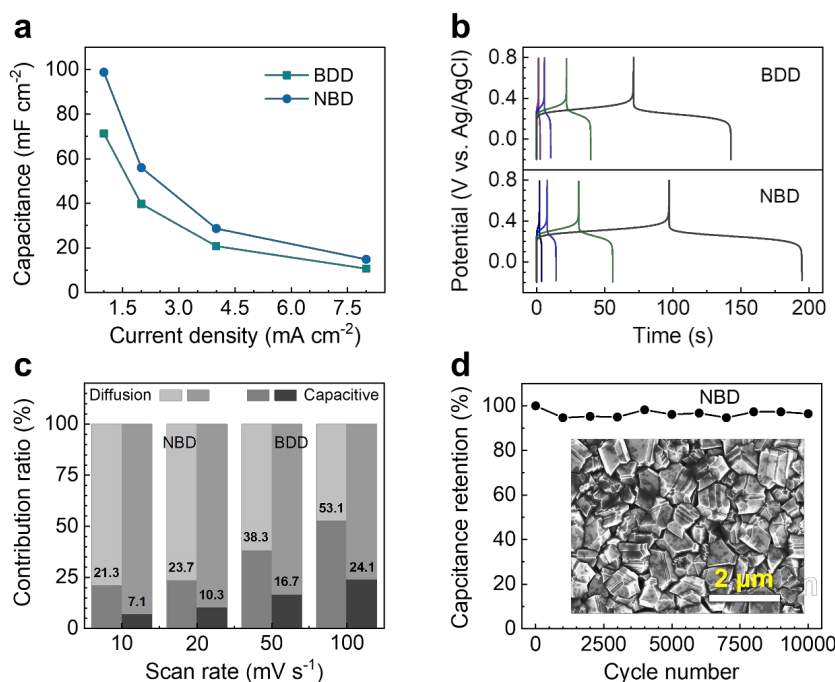


Figure 4. Capacitive performance of the NBD and BDD electrodes in 0.05 M $\text{Fe}(\text{CN})_6^{3-}$ / 1.0 M NaSO_4 : (a) the GCD curves at the current densities of 1, 2, 4, and 8 mA cm^{-2} ; (b) the variation of the specific capacitances with the current densities; (c) the contribution ratios of capacitive and diffusion capacity as a function of scan rates; (d) the capacitance retention at a current density of 8 mA cm^{-2} . The inset shows the SEM image of the post-treated NBD electrode after 10000 GCD cycles.

4. Conclusion

The electrochemistry of nitrogen and boron bi-element incorporated diamond film is explored. The NBD electrode reveals better electrochemical responses in both inner-sphere $[\text{Fe}(\text{CN})_6]^{3-/4-}$ and outer-sphere $[\text{Ru}(\text{NH}_3)_6]^{3+/2+}$ redox systems, when compared

to a BDD electrode. The improved electrochemical performance of the NBD film is related to the enrichment of C=O bonds and the increase amount of sp^2 species on the NBD film. The bigger capacitance of the NBD electrode than that of a BDD mainly stems from that the incorporation of nitrogen and boron atoms into the diamond modulates the surface polarities and the electronic structures of diamond. Moreover, a higher amount of boron atoms in the NBD film is expected than that in the BDD film, due to the "enhanced incorporation" effect of nitrogen in the gas mixture. Such an enhanced capacitance of the NBD electrode extends its potential applications for electrochemical energy storage. Future work has to be conducted on the effect of the densities of incorporated atoms in the NBD film and the surface terminations of the NBD film on the electrochemistry of these bi-element incorporated diamond films. Their further electrochemical energy storage (e.g., for SCs and batteries) and catalytic applications (e.g., for water splitting and CO₂ reduction, nitrogen fixation) can be tried. In summary, this work provides a new electrode material for future electrochemical applications.

Acknowledgements

T. Guo acknowledges the financial support from the China Scholarship Council (No. 201906370017). N. Yang acknowledges funded by the Deutsche Forschungsgemeinschaft (DFG, German Research Foundation) under the project 457444676. B. Yang acknowledges the financial support from the National Natural

Science Foundation of China (Grant No. 51872294). O. Williams acknowledges the financial support of the European Research Council (ERC) Consolidator Grant “SUPERNEMS” under the Project of 647471. Part of this work was performed at the Micro- and Nanoanalytics Facility (MNaF) at the University of Siegen.

References

- [1] A.J. Lucio, R.E. Meyler, M.A. Edwards, J.V. Macpherson, Investigation of sp^2 Carbon Pattern Geometry in Boron-Doped Diamond Electrodes for the Electrochemical Quantification of Hypochlorite at High Concentrations, *ACS sensors* 5(3) (2020) 789-797.
- [2] N. Yang, H. Uetsuka, E. Osawa, C.E. Nebel, Vertically aligned diamond nanowires for DNA sensing, *Angewandte Chemie International Edition* 47(28) (2008) 5183-5185.
- [3] Z. Jian, N. Yang, M. Vogel, S. Leith, A. Schulte, H. Schönherr, T. Jiao, W. Zhang, J. Müller, B. Butz, Flexible Diamond Fibers for High-Energy-Density Zinc-Ion Supercapacitors, *Advanced Energy Materials* (2020) 2002202.
- [4] S. Yu, N. Yang, M. Vogel, S. Mandal, O.A. Williams, S. Jiang, H. Schönherr, B. Yang, X. Jiang, Battery-like supercapacitors from vertically aligned carbon nanofiber coated diamond: design and demonstrator, *Advanced Energy Materials* 8(12) (2018) 1702947.

- 1 [5] S. Yu, J. Xu, H. Kato, N. Yang, A. Schulte, H. Schönherr, X. Jiang, Phosphorus-
2 doped nanocrystalline diamond for supercapacitor application, *ChemElectroChem* 6(4)
3 (2019) 1088-1093.
- 4 [6] M. Tomisaki, S. Kasahara, K. Natsui, N. Ikemiya, Y. Einaga, Switchable product
5 selectivity in the electrochemical reduction of carbon dioxide using boron-doped
6 diamond electrodes, *Journal of the American Chemical Society* 141(18) (2019) 7414-
7 7420.
- 8 [7] K. Natsui, H. Iwakawa, N. Ikemiya, K. Nakata, Y. Einaga, Stable and highly
9 efficient electrochemical production of formic acid from carbon dioxide using diamond
10 electrodes, *Angewandte Chemie* 130(10) (2018) 2669-2673.
- 11 [8] B. Liu, Y. Zheng, H.-Q. Peng, B. Ji, Y. Yang, Y. Tang, C.-S. Lee, W. Zhang
12 Nanostructured and Boron-Doped Diamond as an Electrocatalyst for Nitrogen Fixation,
13 *ACS Energy Letters* 5(8) (2020) 2590-2596.
- 14 [9] P. Nidheesh, G. Divyapriya, N. Oturan, C. Trellu, M.A. Oturan, Environmental
15 applications of boron-doped diamond electrodes: 1. Applications in water and
16 wastewater treatment, *ChemElectroChem* 6(8) (2019) 2124-2142.
- 17 [10] C. Zhang, J. Wang, H. Zhou, D. Fu, Z. Gu, Anodic treatment of acrylic fiber
18 manufacturing wastewater with boron-doped diamond electrode: a statistical approach,
19 *Chemical Engineering Journal* 161(1-2) (2010) 93-98.
- 20 [11] Z. Teukam, J. Chevallier, C. Saguy, R. Kalish, D. Ballutaud, M. Barbé, F. Jomard,
21 A. Tromson-Carli, C. Cytermann, J.E. Butler, Shallow donors with high n-type

1 electrical conductivity in homoepitaxial deuterated boron-doped diamond layers,
2 Nature materials 2(7) (2003) 482-486.

3 [12] T. Yokoya, T. Nakamura, T. Matsushita, T. Muro, Y. Takano, M. Nagao, T.
4 Takenouchi, H. Kawarada, T. Oguchi, Origin of the metallic properties of heavily
5 boron-doped superconducting diamond, Nature 438(7068) (2005) 647-650.

6 [13] P. Lim, F. Lin, H. Shih, V. Ralchenko, V. Varnin, Y.V. Pleskov, S. Hsu, S. Chou,
7 P. Hsu, Improved stability of titanium based boron-doped chemical vapor deposited
8 diamond thin-film electrode by modifying titanium substrate surface, Thin Solid Films
9 516(18) (2008) 6125-6132.

10 [14] E. Brillas, C.A. Mart, Synthetic diamond films: preparation, electrochemistry,
11 characterization, and applications, John Wiley & Sons 2011.

12 [15] Y. Takagi, K. Shiraishi, M. Kasu, H. Sato, Mechanism of hole doping into
13 hydrogen terminated diamond by the adsorption of inorganic molecule, Surface Science
14 609 (2013) 203-206.

15 [16] L.A. Hutton, J.G. Iacobini, E. Bitziou, R.B. Channon, M.E. Newton, J.V.
16 Macpherson, Examination of the factors affecting the electrochemical performance of
17 oxygen-terminated polycrystalline boron-doped diamond electrodes, Analytical
18 chemistry 85(15) (2013) 7230-7240.

19 [17] N. Yang, J.S. Foord, X. Jiang, Diamond electrochemistry at the nanoscale: A
20 review, Carbon 99 (2016) 90-110.

- 1 [18] S. Garcia-Segura, E.V. Dos Santos, C.A. Martínez-Huitle, Role of sp^3/sp^2 ratio on
2 the electrocatalytic properties of boron-doped diamond electrodes: a mini review,
3 *Electrochemistry Communications* 59 (2015) 52-55.
- 4 [19] H.E. Hussein, H. Amari, J.V. Macpherson, Electrochemical synthesis of
5 nanoporous platinum nanoparticles using laser pulse heating: application to methanol
6 oxidation, *ACS Catalysis* 7(10) (2017) 7388-7398.
- 7 [20] D. Guo, R. Shibuya, C. Akiba, S. Saji, T. Kondo, J. Nakamura, Active sites of
8 nitrogen-doped carbon materials for oxygen reduction reaction clarified using model
9 catalysts, *Science* 351(6271) (2016) 361-365.
- 10 [21] Y. Jia, L. Zhang, L. Zhuang, H. Liu, X. Yan, X. Wang, J. Liu, J. Wang, Y. Zheng
11 Z. Xiao, Identification of active sites for acidic oxygen reduction on carbon catalysts
12 with and without nitrogen doping, *Nature Catalysis* 2(8) (2019) 688-695.
- 13 [22] V.N. Mochalin, O. Shenderova, D. Ho, Y. Gogotsi, The properties and applications
14 of nanodiamonds, *Nature nanotechnology* 7(1) (2012) 11-23.
- 15 [23] Y. Lin, D. Su, Fabrication of nitrogen-modified annealed nanodiamond with
16 improved catalytic activity, *ACS nano* 8(8) (2014) 7823-7833.
- 17 [24] Y. Liu, S. Chen, X. Quan, H. Yu, Efficient electrochemical reduction of carbon
18 dioxide to acetate on nitrogen-doped nanodiamond, *Journal of the American Chemical*
19 *Society* 137(36) (2015) 11631-11636.
- 20 [25] H. Wang, Y.-K. Tzeng, Y. Ji, Y. Li, J. Li, X. Zheng, A. Yang, Y. Liu, Y. Gong, L.
21 Cai, Synergistic enhancement of electrocatalytic CO_2 reduction to C_2 oxygenates at

1 nitrogen-doped nanodiamonds/Cu interface, *Nature nanotechnology* 15(2) (2020) 131-
2 137.

3 [26] J. Zhang, Z. Zhao, Z. Xia, L. Dai, A metal-free bifunctional electrocatalyst for
4 oxygen reduction and oxygen evolution reactions, *Nature nanotechnology* 10(5) (2015)
5 444-452.

6 [27] C. Zhang, X. Wang, Q. Liang, X. Liu, Q. Weng, J. Liu, Y. Yang, Z. Dai, K. Ding,
7 Y. Bando, Amorphous phosphorus/nitrogen-doped graphene paper for ultrastable
8 sodium-ion batteries, *Nano letters* 16(3) (2016) 2054-2060.

9 [28] Y. Zhao, N. Yang, H. Yao, D. Liu, L. Song, J. Zhu, S. Li, L. Gu, K. Lin, D. Wang
10 Stereodefined codoping of sp²-N and S atoms in few-layer graphdiyne for oxygen
11 evolution reaction, *Journal of the American Chemical Society* 141(18) (2019) 7240-
12 7244.

13 [29] Y. Liu, Y. Zhang, K. Cheng, X. Quan, X. Fan, Y. Su, S. Chen, H. Zhao, Y. Zhang,
14 H. Yu, Selective electrochemical reduction of carbon dioxide to ethanol on a boron-and
15 nitrogen-Co-doped nanodiamond, *Angewandte Chemie* 129(49) (2017) 15813-15817.

16 [30] Y. Liu, S. Chen, X. Quan, H. Yu, H. Zhao, Y. Zhang, G. Chen, Boron and nitrogen
17 codoped nanodiamond as an efficient metal-free catalyst for oxygen reduction reaction,
18 *The Journal of Physical Chemistry C* 117(29) (2013) 14992-14998.

19 [31] N. Yang, S. Yu, J.V. Macpherson, Y. Einaga, H. Zhao, G. Zhao, G.M. Swain, X.
20 Jiang, Conductive diamond: synthesis, properties, and electrochemical applications,
21 *Chemical Society Reviews* 48(1) (2019) 157-204.

- 1 [32] J. Xu, N. Yang, S. Heuser, S. Yu, A. Schulte, H. Schönherr, X. Jiang, Achieving
2 ultrahigh energy densities of supercapacitors with porous titanium carbide/boron-doped
3 diamond composite electrodes, *Advanced Energy Materials* 9(17) (2019) 1803623.
- 4 [33] J. Hees, A. Kriele, O.A. Williams, Electrostatic self-assembly of diamond
5 nanoparticles, *Chemical Physics Letters* 509(1-3) (2011) 12-15.
- 6 [34] O.A. Williams, Nanocrystalline diamond, *Diamond and Related Materials* 20(5-6)
7 (2011) 621-640.
- 8 [35] O.A. Williams, O. Douhéret, M. Daenen, K. Haenen, E. Ōsawa, M. Takahashi,
9 Enhanced diamond nucleation on monodispersed nanocrystalline diamond, *Chemical*
10 *Physics Letters* 445(4-6) (2007) 255-258.
- 11 [36] T.S. Mathis, N. Kurra, X. Wang, D. Pinto, P. Simon, Y. Gogotsi, Energy storage
12 data reporting in perspective—guidelines for interpreting the performance of
13 electrochemical energy storage systems, *Advanced Energy Materials* 9(39) (2019)
14 1902007.
- 15 [37] W. Lu, J. Shen, P. Zhang, Y. Zhong, Y. Hu, X.W. Lou, Construction of CoO/Co-
16 Cu-S Hierarchical Tubular Heterostructures for Hybrid Supercapacitors, *Angewandte*
17 *Chemie International Edition* 58(43) (2019) 15441-15447.
- 18 [38] T. Brezesinski, J. Wang, S.H. Tolbert, B. Dunn, Ordered mesoporous α -MoO₃
19 with iso-oriented nanocrystalline walls for thin-film pseudocapacitors, *Nature materials*
20 9(2) (2010) 146-151.

- 1 [39] T. Liu, D. Raabe, Influence of nitrogen doping on growth rate and texture evolution
2 of chemical vapor deposition diamond films, *Applied Physics Letters* 94(2) (2009)
3 021119.
- 4 [40] K.N. Kudin, B. Ozbas, H.C. Schniepp, R.K. Prud'Homme, I.A. Aksay, R. Car,
5 Raman spectra of graphite oxide and functionalized graphene sheets, *Nano letters* 8(1)
6 (2008) 36-41.
- 7 [41] J.-C. Arnault, X-ray Photoemission Spectroscopy applied to nanodiamonds: From
8 surface chemistry to in situ reactivity, *Diamond and Related Materials* 84 (2018) 157-
9 168.
- 10 [42] J. Xu, Y. Yokota, R.A. Wong, Y. Kim, Y. Einaga, Unusual electrochemical
11 properties of low-doped boron-doped diamond electrodes containing sp^2 carbon,
12 *Journal of the American Chemical Society* 142(5) (2020) 2310-2316.
- 13 [43] O.A. Williams, Ultrananocrystalline diamond for electronic applications,
14 *Semiconductor science and technology* 21(8) (2006) R49.
- 15 [44] P. Achatz, O.A. Williams, P. Bruno, D. Gruen, J. Garrido, M. Stutzmann, Effect
16 of nitrogen on the electronic properties of ultrananocrystalline diamond thin films
17 grown on quartz and diamond substrates, *Physical Review B* 74(15) (2006) 155429.
- 18 [45] Z.J. Ayres, A.J. Borrill, J.C. Newland, M.E. Newton, J.V. Macpherson, Controlled
19 sp^2 functionalization of boron doped diamond as a route for the fabrication of robust
20 and Nernstian pH electrodes, *Analytical chemistry* 88(1) (2016) 974-980.

- 1 [46] S. Yu, N. Yang, H. Zhuang, S. Mandal, O.A. Williams, B. Yang, N. Huang, X.
2 Jiang, Battery-like supercapacitors from diamond networks and water-soluble redox
3 electrolytes, *Journal of Materials Chemistry A* 5(4) (2017) 1778-1785.
- 4 [47] Z. Ling, Z. Wang, M. Zhang, C. Yu, G. Wang, Y. Dong, S. Liu, Y. Wang, J. Qiu,
5 Sustainable synthesis and assembly of biomass-derived B/N co-doped carbon
6 nanosheets with ultrahigh aspect ratio for high-performance supercapacitors, *Advanced*
7 *functional materials* 26(1) (2016) 111-119.
- 8 [48] Z.S. Wu, A. Winter, L. Chen, Y. Sun, A. Turchanin, X. Feng, K. Müllen, Three-
9 dimensional nitrogen and boron co-doped graphene for high-performance all-solid-
10 state supercapacitors, *Advanced Materials* 24(37) (2012) 5130-5135.

11

Supporting Information

Electrochemistry of Nitrogen and Boron

Bi-element Incorporated Diamond Films

Tianxiao Guo,^a Nianjun Yang,^{a*} Bing Yang,^b Anna Schulte,^c Qun Jin,^a Ulrike Koch,^d
Rainer Bornemann,^e Soumen Mandal,^f Carsten Engelhard,^d Oliver A. Williams,^f
Holger Schönherr,^c and Xin Jiang^{a, *}

^a Institute of Materials Engineering, University of Siegen, Siegen 57076, Germany

^b Shenyang National Laboratory for Materials Science, Institute of Metal Research
(IMR), Chinese Academy of Science (CAS), No. 72 Wenhua Road, Shenyang
110016, China

^c Physical Chemistry I, Department of Chemistry and Biology and Research Center of
Micro and Nanochemistry and Engineering (Cμ), University of Siegen, Siegen 57075,
Germany

^d Analytical Chemistry, Department of Chemistry and Biology and Research Center
of Micro and Nanochemistry and Engineering (Cμ), University of Siegen, Siegen
57075, Germany

^e Institute for High Frequency and Quantum Electronics, School of Science and
Technology, University of Siegen, Siegen, Siegen 57076, Germany

^f School of Physics and Astronomy, Cardiff University, Cardiff CF24 3AA, UK

Supporting Tables

Table S1. CVD growth parameters of the boron-doped diamond (BDD) films as well as the nitrogen and boron bi-element incorporated diamond (NBD) films.

	BDD	NBD
Incubation		
Forward power (kW)	4.8	4.8
Chamber pressure (Torr)	45	45
Duration times (min)	7	7
CH ₄ (sccm)	15	15
H ₂ (sccm)	185	82
TMB (sccm) [*]	0.22000	0.42000
N ₂ (sccm)		3
Growth		
Forward power (kW)	4.8	4.8
Chamber pressure (Torr)	45	45
Duration times (min)	1435	1203
CH ₄ (sccm)	3	3
H ₂ (sccm)	277	254
TMB (sccm)	20	40
N ₂ (sccm)		3

^{*} The TMB flow has been calculated based on total flow of gas mix containing 2000ppm TMB diluted in H₂.

Formatted: Font: (Default)TimesNew Roman, Bold

Formatted: Font: (Default)TimesNew Roman, Bold

Table S2. Relative abundance of the carbon components in the BDD and NBD films.*

	sp ² C	sp ³ C	C-O	C=O	C-N	sp ² C/sp ³ C
NBD	3.7	31.0	34.0	28.9	2.4	11.9
BDD	2.0	52.0	32.3	13.6		3.8

* These atomic ratios were estimated from their high resolution C1s XPS spectra

Supporting Figures

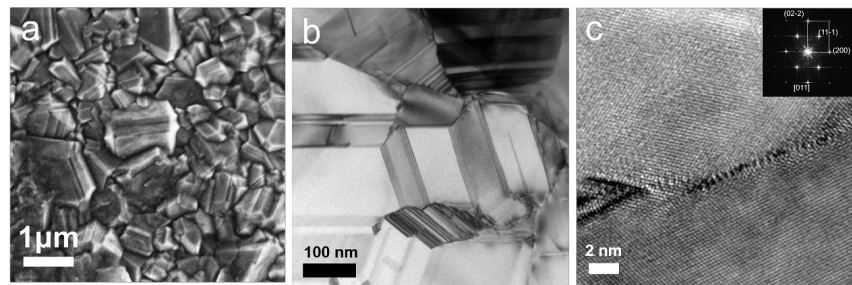


Figure S1. (a) SEM, (b) low-magnification TEM and (c) HRTEM images of the BDD film. The inset in (c) is the corresponding fast Fourier transformation (FFT) of the HRTEM image.

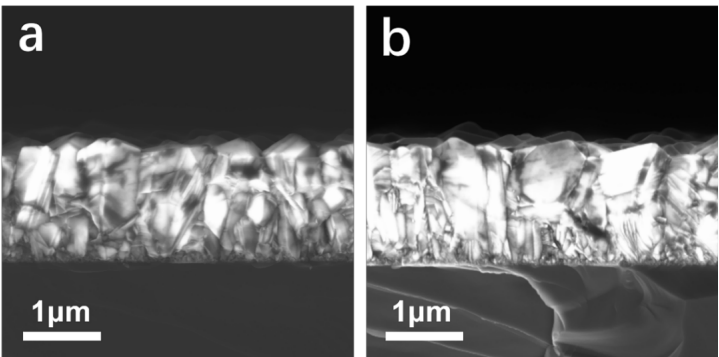


Figure S2. The cross-sectional SEM images of the (a) NBD and (b) BDD films.

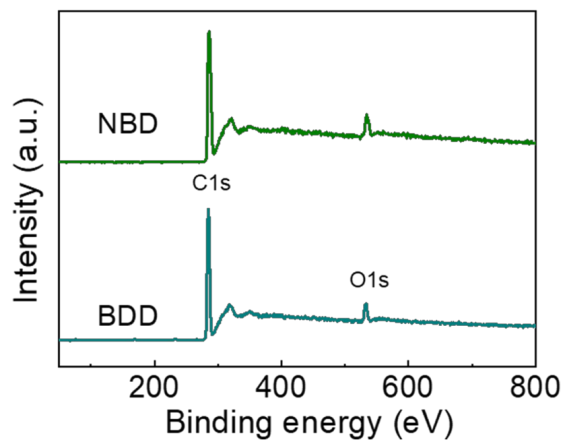


Figure S3. XPS survey spectra for the NBD and BDD films.

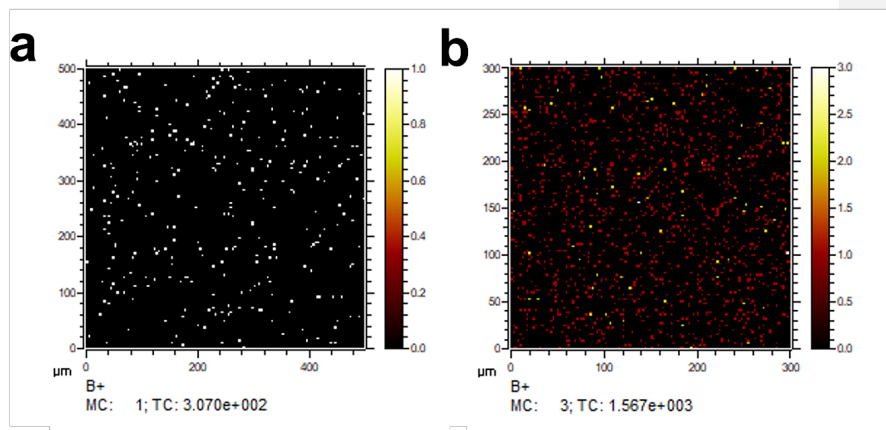


Figure S4. SIMS mapping of boron atoms doped in the BDD film (a) direct and (b) after 30 sec sputtering with Argon for cleaning the surface in the positive mode (MC max counts per pixel, TC total counts).

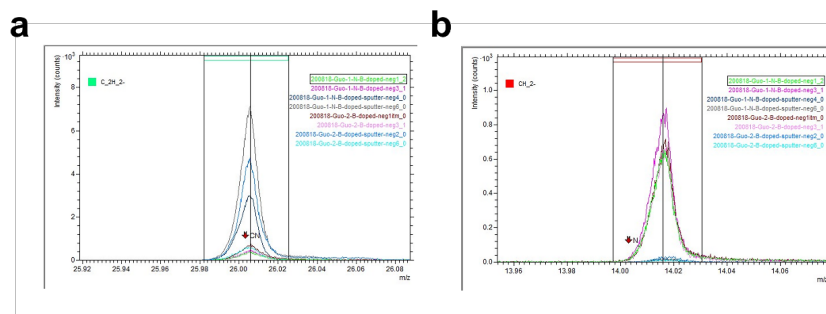


Figure S5. Spectra of the (a) NBD and (b) BDD films in the negative mode. The m/z ratios of N, CH₂, CN, and C₂H₂ are 14,003, 14,0162, 26,0036 and 26,0162, respectively.

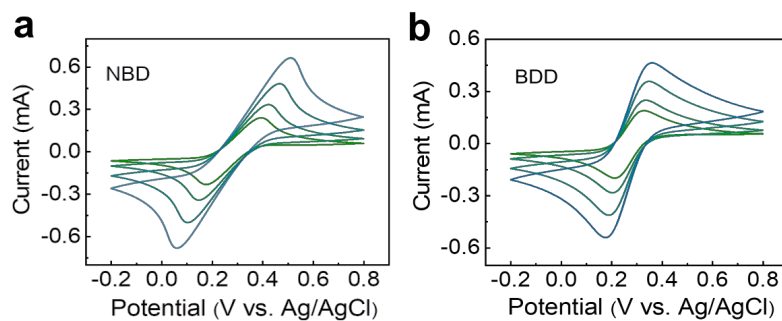


Figure S6. CVs of 0.05 M Fe(CN)₆^{3-/4-} in 1.0 M NaSO₄ on the (a) NBD and (b) BDD electrodes at the scan rates of 100, 50, 20, and 10 mV s⁻¹.

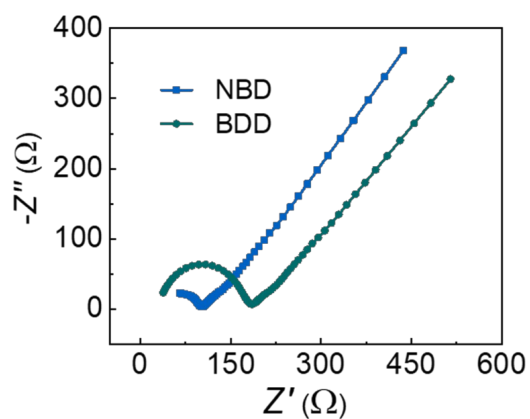


Figure S7. Nyquist plots of the NBD and BDD electrodes in 1.0 M NaSO₄ solution containing 0.05 M Fe(CN)₆^{3-/4-}.

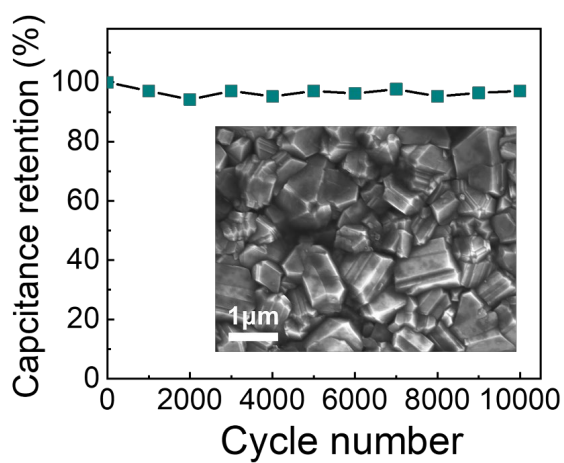


Figure S8. Capacitance retention of a BDD electrode at a current density of 8 mA cm⁻². The inset shows the SEM image of a BDD electrode after 10000 GCD cycles.